A Prime-Boost Vaccination Approach Induces Lung Resident Memory CD8$^+$ T Cells Derived from Central Memory T Cells That Prevent Tumor Lung Metastasis

Haoran Xu[1,2,3], Ming Yue[1,3,4], Runhong Zhou[1,2,3], Pui Wang[2,3], Michael Yik-Chun Wong[1,2,3], Jinlin Wang[1,2,3], Huarong Huang[1,2,3], Bohao Chen[1,2,3], Yufei Mo[1,2,3], Rachel Chun-Yee Tam[2,3], Biao Zhou[1,2,3], Zhenglong Du[1,2,3], Haode Huang[1,2,3], Li Liu[1,2,3], Zhiwu Tan[1,2,3], Kwok-Yung Yuen[2,3,5], Youqiang Song[4], Honglin Chen[2,3,5], and Zhiwei Chen[1,2,3,5]

ABSTRACT

Memory T cells play a key role in immune protection against cancer. Vaccine-induced tissue-resident memory T (T_{RM}) cells in the lung have been shown to protect against lung metastasis. Identifying the source of lung T_{RM} cells can help to improve strategies, preventing tumor metastasis. Here, we found that a prime-boost vaccination approach using intramuscular DNA vaccine priming, followed by intranasal live-attenuated influenza-vectored vaccine (LAIV) boosting induced higher frequencies of lung CD8$^+$ T_{RM} cells compared with other vaccination regimens. Vaccine-induced lung CD8$^+$ T_{RM} cells, but not circulating memory T cells, conferred significant protection against metastatic melanoma and mesothelioma. Central memory T (T_{CM}) cells induced by the DNA vaccination were major precursors of lung T_{RM} cells established after the intranasal LAIV boost. Single-cell RNA sequencing analysis indicated that transcriptional reprogramming of T_{CM} cells for differentiation into T_{RM} cells in the lungs started as early as day 2 post the LAIV boost. Intranasal LAIV altered the mucosal microenvironment to recruit T_{CM} cells via CXCR3-dependent chemotaxis and induced CD8$^+$ T_{RM}-associated transcriptional programs. These results identified T_{CM} cells as the source of vaccine-induced CD8$^+$ T_{RM} cells that protect against lung metastasis.

Significance: Prime-boost vaccination shapes the mucosal microenvironment and reprograms central memory T cells to generate lung resident memory T cells that protect against lung metastasis, providing insights for the optimization of vaccine strategies.

Introduction

Host cellular immunity involves various types of T cells in tissue compartments affected, providing immune surveillance against cancer (1). Memory T cells including circulating memory T (T_{CIRM}) cells and non-recirculating tissue-resident memory T (T_{RM}) cells are critical for prolonged immune protection. T_{CIRM} cells can be further classified into central memory T cells (T_{CM}), effector memory T cells (T_{EM}), T memory stem cells (T_{SCM}), and long-lived effector T cells (T_{LLEC}; refs. 2–5) T_{CIRM} cells may migrate throughout the circulation, whereas T_{RM} cells persist long-term in organ and mucosal tissues (6) and display frontline cytotoxic effects against tumor progression.

Vaccine-induced lung T_{RM} cells have been suggested for mediating better protection against multiple respiratory infections (7). Since the coronavirus disease 2019 (COVID-19) outbreak, various intranasal vaccines have been tested to induce or further boost the lung T_{RM} cells. We and others showed that the heterologous intramuscular prime-intranasal boost vaccine regimen could elicit significantly enhanced lung CD8$^+$ T_{RM} cells for SARS-CoV-2 protection (8, 9). Similar prime-boost regimens can also mediate melanoma lung metastasis protection (10, 11). Although lung CD8$^+$ T_{RM} cells are associated with better clinical outcomes (12), how to elicit abundant and long-lasting CD8$^+$ T_{RM} cells for lung cancer metastasis protection remains challenging (13).

To understand the source of vaccine-induced lung T_{RM} cells, it is necessary to reveal the differentiation and expansion of primed memory CD8$^+$ T cells after mucosal boost vaccination (14). Previous studies have illustrated that T_{CM} cells retain stemness to repopulate into heterosubtypic memory T cells, with substantial capacity to differentiate into skin T_{RM} cells (15–17). T_{EM} cells may replenish lung T_{RM} cells during influenza reinfection and vaccination (18). On the contrary, other studies argued that T_{EM} cells gave rise to only a small fraction of T_{RM} cells maintained within the lung interstitium (19, 20). T_{CIRM} cells identified in both lung tissue and circulation were also suggested as a potential source of lung T_{RM}-cell induction (1).

[1]AIDS Institute, School of Clinical Medicine, Li Ka Shing Faculty of Medicine, The University of Hong Kong, Hong Kong, People's Republic of China. [2]Department of Microbiology, School of Clinical Medicine, Li Ka Shing Faculty of Medicine, The University of Hong Kong, Hong Kong, People's Republic of China. [3]State Key Laboratory of Emerging Infectious Diseases, The University of Hong Kong, Hong Kong, People's Republic of China. [4]School of Biomedical Science, Li Ka Shing Faculty of Medicine, The University of Hong Kong, Hong Kong, People's Republic of China. [5]Center for Virology, Vaccinology and Therapeutics, Hong Kong, People's Republic of China.

H. Xu, M. Yue, R. Zhou, and P. Wang contributed equally to this article.

Corresponding Author: Zhiwei Chen, AIDS Institute and Department of Microbiology, Li Ka Shing Faculty of Medicine, The University of Hong Kong, L5-45, 21 Sassoon Road, Pokfulam, Hong Kong, People's Republic of China. E-mail: zchenai@hku.hk

Cancer Res 2024;84:3173–88

doi: 10.1158/0008-5472.CAN-23-3257

In this study, we investigated the source of lung T_{RM} cells in the systemic prime-mucosal boost immunization strategy (9). Using the heterologous intramuscular DNA vaccine prime and live-attenuated influenza viral–vectored vaccine (LAIV) intranasal boost regimen, we demonstrated that vaccine-elicited lung $CD8^+$ T_{RM} cells, rather than T_{CIRM} cells, mainly mediated the protection against melanoma and mesothelioma lung metastasis. Moreover, the systemic vaccine-primed T_{CM} cells were the major precursors of lung T_{RM} cells generated after the intranasal boost vaccination. Single-cell RNA sequencing (scRNA-seq) analysis revealed that the T_{CM}- to lung T_{RM}-cell differentiation was initiated as early as day 2 post the intranasal booster vaccination. The intercellular communication induced the T_{RM}-associated transcriptional heterogenicity in the early reactivation stage, prior to the phenotype switch of T_{CM} cells. These data collectively demonstrated a significant role of $CD8^+$ T_{RM} cells in protecting melanoma and mesothelioma lung metastasis and revealed the underlying mechanism of lung $CD8^+$ T_{RM}-cell induction by the heterologous systemic prime-intranasal boost vaccination regimen.

Materials and Methods

Mice

Six-to-ten weeks old male and female BALB/c (RRID:MGI 2683685), C57BL/6 (RRID:IMSR_JAX:000664), and OT-I mice (RRID:IMSR_JAX:003831) were obtained from the University of Hong Kong Centre for Comparative Medicine Research. B6.SJL-Ptprca Pepcb/BoyJ (CD45.1) mice (RRID:IMSR_JAX:002014), kindly provided by Prof. Lu Liwei (Department of Pathology, HKU LKS Faculty of Medicine, Hong Kong), and CXCR3 knockout ($CXCR3^{-/-}$) mice, kindly provided by Prof. Man Kwan (Department of Surgery, HKU LKS Faculty of Medicine), were bred in the University of Hong Kong Centre for Comparative Medicine Research for research.

Ethics

All animals were housed in Biosafety Level-2 pathogen-free conditions at the University of Hong Kong Centre for Comparative Medicine Research. All animal studies were approved by the Committee on the Use of Live Animals in Teaching and Research, The University of Hong Kong.

Cell lines and vaccines

Canine MDCK cells (RRID:CVCL_0422) were maintained in the Eagle's minimum essential medium (MEM) with 10% fetal bovine serum (FBS), 100 U/mL penicillin, and 100 μg/mL streptomycin sulfate (P/S). HEK293T cells (RRID:CVCL_0063) were cultured in DMEM with the same amount of FBS and P/S. Both cell lines were obtained from ATCC for influenza-vectored vaccine construction. AB1 and B16F10 cells expressing HIV-Gag, kindly provided by Dr. Tan Zhiwu and authenticated by Western blot, were cultured in DMEM supplemented with 10% FBS, 1% P/S, and 1 μg/mL puromycin. DNA vaccine expressing HIV-1 Gag Mosaic immunogen (DNA-Gag) was constructed as previously reported (21). LAIV-CA04-Gag and LAIV-HK68-Gag were constructed as previously described (22). In brief, gene segments from H1N1 virus A/California/04/2009 or H3N2 A/HK/1/1968 were cloned into pHW2000 plasmids separately. HIV-Gag mosaic gene segment was inserted into the site of NS1 deletion. The size of full-length Gag Mosaic antigen exceeded the capacity of the NS1 deletion segment, which leads to unsuccessful vaccine packaging. We, therefore, separated it into Gag Mosaic 1 segment and Gag Mosaic 2 segment, 1089 bp for each, and cloned into the deleted NS1 segment for generating LAIV-CA04-Gag Mosaic-1, LAIV-CA04-Gag Mosaic-2 (termed as LAIV-CA04-Gag jointly), LAIV-HK68-Gag-1, and LAIV-HK68-Gag-2 (termed as LAIV-HK68-Gag jointly). Eight plasmids coding LAIV-CA04-Gag or LAIV-HK68-Gag segments were cotransfected into HEK293T cells and cultured at 33°C for 48 hours to generate P0 vaccine. P0 vaccine was subsequently passaged in embryonated chicken eggs at 33°C for 48 hours to rescue the P1 vaccine for animal experiments. Vaccines were titrated by plaque assay in MDCK cells as previously described (22). Cells were used in this study between passages 2 and 10. All cell lines were maintained at 37°C with 21% O_2 and 5% CO_2, and *Mycoplasma* PCR detection was performed before use.

Plaque assay

Plaque assay was applied for LAIV-based vaccine titration (22). LAIV harvested from embryonated eggs were 10-fold serially diluted with PBS and incubated with confluent MDCK cells in a six-well plate for 1 hour at 33°C. The supernatant was then removed, and cells were subsequently covered with 1% agarose in MEM for further 3 days of incubation at 33°C. Application of 4% PFA for 1-hour fixation before the removal of agarose gels was done, and plaques were visualized by adding 1% crystal violet.

Animal immunization, B16F10-GAG, and AB1-GAG tumor challenge

Six-to-ten weeks old BALB/c or C57BL/6 mice in both genders received DNA vaccination by intramuscular electroporation (i.m./EP) with 50 μg DNA-Gag. The voltage of electroporation was 60 V using the TERESA DNA Delivery Device (Shanghai Teresa Healthcare Sci-Tech Co., Ltd.). For the influenza-vectored vaccine immunization, mice were anesthetized by intraperitoneally (i.p.) injecting the mixture of ketamine/xylazine solution (60 and 10 mg/kg). A total of 1×10^6 PFU LAIV-CA04-Gag or LAIV-HK68-Gag were prepared in 40 μL PBS for intranasal inoculation (i.n.) and in 100 μL PBS for the intramuscular immunization. For the tumor challenge, B16F10-Gag cells were harvested and single-cell suspensions of 1×10^6 cells in 200 μL PBS were i.v. injected into immunized C57BL/6 mice. Luciferase-expressing tumor growth kinetics was screened in the IVIS Spectrum System (PerkinElmer), and luminescent intensity was measured within the regions of interest (ROI). Bioluminescence intensity within the ROI was presented as photons/s/cm^2/sr. Acquired data were analyzed with Live Imaging software (version 4.0; PerkinElmer). After reaching the humane endpoint, lungs were collected and fixed in Fekete's solution for lung metastasis nodule counting. In mesothelioma challenge experiments, AB1-Gag cells were harvested, and single-cell suspensions of 1×10^6 cells in 200 μL PBS were i.v. injected into immunized BALB/c mice.

Antibodies and flow cytometry

Following anti-mouse antibodies were purchased and used at 1:100 dilution: anti-mouse CD3 (PerCP-Cy5.5, Clone: 17A2, BioLegend, cat. #100218, RRID:AB_1595492), anti-mouse CD8α (BV785, Clone: 53-6.7, BioLegend, cat. #100750, RRID:AB_2562610), anti-mouse CD4 (V450, Clone: RM 4-5, eBioscience, cat. #48-0042-82, RRID: AB_2016674), anti-mouse CD103 (BV421, Clone: 2E7, BioLegend, cat. #121422, RRID:AB_2562901), anti-mouse CD69 (APC, Clone: H1.2F3, BioLegend, cat. #104514, RRID:AB_492843), anti-mouse CD62L (FITC, Clone: MEL-14, BioLegend, cat. #104406, RRID: AB_313093), anti-mouse CD44 (APC-Fire750, Clone: IM7, BioLegend,

cat. #103062, RRID:AB_2616727), anti-mouse IFNγ (Alexa Fluor 488, Clone: XMG1.2, BioLegend, cat. #505813, RRID:AB_493312), anti-mouse TNFα (PE, Clone: MP6-XT22, BioLegend, cat. #506306, RRID: AB_315427), anti-mouse IL2 (FITC, Clone: JES6-5H4, BioLegend, cat. #503806, RRID:AB_315300), anti-mouse CD45.1 (APC, Clone: A20, BioLegend, cat. #110714, RRID:AB_313503), anti-mouse CD45.2 (PE/Cy7, Clone: 104, BioLegend, cat. #109830, RRID:AB_1186098), anti-mouse CD11b (APC, Clone: M1/70, BioLegend, cat. #101212, RRID: AB_312795), anti-mouse Ly6G (PE, Clone: 1A8, BD Biosciences, cat. #551461, RRID:AB_394208), anti-mouse Ly6C (APC-Fire750, Clone: HK1.4, BioLegend, cat. #128046, RRID:AB_2616731), anti-mouse F4/80 (PerCP-Cy5.5, Clone: BM8, eBioscience, cat. #45-4801-82, RRID: AB_914345), anti-mouse PD-1 (PE/Cy7, Clone: 29F.1A12, BioLegend, cat. #135216, RRID:AB_10689635), anti-mouse NK1.1 (PerCP-Cy5.5, Clone: PK136, BioLegend, cat. #108728, RRID:AB_2132705), anti-mouse CD49b (APC, Clone: DX5, eBioscience, cat. #17-5971-82, RRID: AB_469485), anti-mouse Foxp3 (APC, Clone: MF-14, BioLegend, cat. #126406, RRID:AB_1089113), anti-mouse CD25 (PECy7, Clone: PC61.5, eBioscience, cat. #25-0251-82, RRID:AB_469608), anti-mouse CXCR3 (APC, Clone: CXCR3-173, BioLegend, cat. #126512, RRID: AB_1088993), anti-mouse CCR5 (PECy7, Clone: HM-CCR5, BioLegend, cat. #107018, RRID:AB_2617013). Zombie Aqua Fixable Viability Kit (Biolegend, cat. #423102) was used at 1:100 dilution for live cell staining. For tetramer staining assay, PE-conjugated H-2Kd HIV-1 Gag (AMQMLKETI) MHC class I tetramer (MBL), APC-conjugated H-2Kd influenza nucleoprotein (NP) MHC class I tetramer (MBL), and PE-conjugated H-2Kb OVA (SIINFEKL) MBL were cultured with cells isolated from the mouse tissues at 1:50 dilution at room temperature for 15 minutes, and other surface marker antibodies were added at designated dilution and stained at 4°C for 30 minutes. For the intracellular cytokine staining (ICS) assay, cells isolated from tissues were stimulated with RPMI 1640 medium containing 1 μg/mL of HIV-1 Gag peptide pool (15-mer overlapping by 11, spanning the HIV-1 clade A, B, and C Gag protein) or no peptide as the background control. After 3 hours, brefeldin A (BFA) was added and cells were incubated at 37°C overnight. Cells were subsequently washed with FACS buffer (PBS containing 2% FBS) and stained with surface markers for 30 minutes at 4°C. Cells were then fixed with fixation/permeabilization solution (BD Biosciences) at 4°C for 30 minutes and then stained with intracellular cytokine antibodies in BD Perm/Wash Buffer overnight at 4°C. Cells were then washed and resuspended in FACS buffer. Stained samples were acquired with BD FACS Aria III cell sorter (BD Biosciences) and the data were analyzed by FlowJo V10 (RRID:SCR_008520). Cytokine production frequency was calculated by subtracting the designated sample with no peptide control.

Generation of OVA-specific circulating memory T cells and adoptive transfer

To generate OVA-specific T_{EM} and T_{CM} cells, spleen and lymph nodes from naïve CD45.2$^+$ OT-I mice were harvested. Isolated single cells proceeded to CD8$^+$ T-cell isolation using the mouse CD8a$^+$ T Cell Isolation Kit under the manufacturer's instructions. Enriched naïve OVA-specific CD8$^+$ T (OT-1) cells were adoptively transferred into CD45.1$^+$ transgenic recipients. About 3×10^7 naïve OT-I cells were isolated from six donor mice and subsequently i.v. transferred into 24 recipient mice (1.25×10^6 naïve OT-I cells per mouse). Donor mice were six-to-eight weeks old male or female and the recipient mice were six-to-eight weeks old males. Recipients were vaccinated with 50 μg DNA-OVA in 100 μL PBS by i.m./EP injection on the first, fourth, and seventh day post-adoptive transfer to adequately activate transferred naïve OT-I cells (23). Spleen and lymph nodes were collected at 3 weeks post-final DNA-OVA vaccination (the same time for the booster vaccination in the prime-boost vaccination regimen) to isolate lymphocytes. To sort the T_{EM} and T_{CM} cells for adoptive transfer, isolated lymphocytes were stained with anti-mouse-CD3e, anti-mouse-CD8, anti-mouse-CD4, anti-mouse-CD44, anti-mouse-CD62L, anti-mouse-CD45.1, anti-mouse-CD45.2, and Zombie aqua. Samples were acquired by FACS Aria III Cell Sorter for two-way cell sorting according to the manufacturer's instructions. For memory T-cell adoptive transfer, 10^5 sorted OVA-specific T_{EM} or T_{CM} cells were adoptively transferred into different DNA-OVA primed (3 weeks before adoptive transfer) CD45.1$^+$ transgenic recipients, respectively. Cells isolated from 24 memory T-cell donors were equally transferred into seven T_{EM} cell recipients and seven T_{CM} cell recipients.

Parabiosis surgery

Six to eight weeks C57BL/6 mice of the same gender and similar body weight were paired for parabiosis surgery (24). The joint skin was disinfected with 70% alcohol before surgery. Using a sharp scissor, the shaved sides of each animal were performed with longitudinal skin incisions starting at 0.5 cm above the elbow to 0.5 cm below the knee joint. Following the incision, the skin was gently detached from the subcutaneous fascia to create 0.5 cm of free skin. This separation was performed along the entire incision. The left olecranon of one animal was attached to the right olecranon of the other. Both olecranon and knee joints were distinguishable following the skin incision. To facilitate the joining, the elbow of the first mouse was bent, and the needle of the nonabsorbable 5-0 suture was passed under the olecranon. Similarly, the elbow of the second mouse was bent and the same suture was passed under it. The joints were attached tightly by a double surgical knot. The knee joints were connected following the same procedure. Following the attachment of the joints, the skin of the two animals was connected with a suture starting ventrally from the elbow toward the knee. The continuity of the suture was verified and confirmed the lack of openings. Animals were kept on a heated pad until recovery.

Tissue total RNA extraction and chemokine detection

For chemokine RNA detection, half of the lungs collected from vaccinated mice were homogenized using TissueRuptor II (QIAGEN), and total RNA was extracted using RNeasy Mini Kit (QIAGEN). cDNA was prepared from 1 μg of RNA using PrimeScript II 1st Strand cDNA Synthesis Kit (Takara). One-Step TB Green PrimeScript RT-PCR Kit II (Takara) was used for the quantitative real-time PCR (qRT-PCR) assay. qRT-PCR assay was performed on ViiA 7 Real-Time PCR System (Thermo Scientific). The primers for chemokines in qRT-PCR assay were listed in Supplementary Table S1.

Histopathology staining

Lung tissues from melanoma-challenged mice were obtained at the endpoint and fixed by zinc formalin. Thereafter, fixed tissues were embedded in paraffin as tissue blocks. Tissue blocks were then processed into section slides at 4 μm thickness. Then slides collected from the tumor challenge experiment were stained with

hematoxylin and eosin and subjected to inspection under Zeiss LSM 980 confocal microscope and processed with ZEISS imaging software.

ELISA for chemokine detection

For chemokine protein detection, half of the lungs collected from vaccinated mice were homogenized using TissueRuptor II (QIAGEN). We utilized LEGENDplex Mouse Proinflammatory Chemokine Panel (cat. #740451) to measure the protein level of CXCL9 and CXCL10.

T-cell depletion assays

At day 30 post boost vaccination, V1 vaccinated mice were i.p. injected with 500 μg anti-CD8 mAb (YTS169.4) and/or anti-CD4 mAb (YTS191.1) in 200 μL PBS for one time (25). T-cell depletion outcomes were confirmed by FACS analysis of peripheral blood $CD4^+$ or $CD8^+$ T cells. Naïve mice were included as the negative control, and V1 vaccinated mice served as the positive control. Melanoma tumor challenge was performed 30 days post T-cell depletion.

Single-cell RNA sequencing

Tissues were harvested at designated time points from mice that received different vaccination ($n = 3$), and subsequently proceeded to the red blood cell lysis. Dead Cell Removal Kit (Miltenyi Biotec) was utilized to remove dead cells before scRNA-seq sample submission. The same tissue harvested from three individual mice in the same group was combined into one scRNA-seq sample for subsequent sequencing and analysis to ensure the proper experimental duplication. Single-cell encapsulation and cDNA libraries were performed using the 10× Chromium Next GEM Single Cell 3′ Reagent Kit v3.1 and Chromium Next GEM Chip G Single Cell Kit. Purified libraries were sequenced on an Illumina Novaseq 6000 sequencer with 151 bp paired-end reads.

Quality control, integration, and clustering

The raw FASTQ files were mapped to the 10× Genomics prebuilt mm10 genome reference (2020-A), and the raw count matrices were generated with Cell Ranger v6.0.2 (26). Quality control and analysis procedures were performed using Seurat v4.3.0 (RRID: SCR_007322; ref. 27) based on R v4.1.2. The ambient RNA in the data was evaluated and removed using Soup X v1.5.2 (28), and Scrublet (29) was used to remove doublets. To reduce the initial noise, cells with fewer than 500 genes expressed, 1,000 total UMI counts, and a proportion of mitochondrial gene expression accounting for more than 10% were excluded from the subsequent analysis. The samples were normalized (Normalize Data function in Seurat) using default parameters and were integrated based on a set of 4,000 most variable expression genes (Find Variable Features function in Seurat) across cells using Harmony (30). Elbow plots (Elbow Plot function in Seurat) were created to determine the best dimension parameter. Uniform Manifold Approximation and Projection (UMAP; ref. 31) dimensionality reduction was performed using the top 30 principal components. The cell group division was obtained at the appropriate resolution with the Find Clusters function in Seurat. The specific cell type of each cell population was determined by comparing markers identified in previous literature (32–34). Samples collected from lung, mediastinal lymph node (MLN), and spleen were integrated and clustered separately. For the integration of $CD8^+$ T cells, cells satisfying Cd8a/b>0 and Cd3d/e>0 in each sample were extracted and integrated together.

Differential gene expression analysis

Differentially expressed genes (DEG) were evaluated using MAST (35). *P*-values were adjusted using the Bonferroni correction based on the total number of genes in the dataset. To identify DEGs, the following criteria were used: a log fold change threshold of 0.25, an adjusted *P*-value less than 0.05, and presence in at least 10% of cells in the cluster. Kinetic changes across different immunization approaches and cell subpopulations were evaluated using the R package (https://github.com/ctlab/fgsea).

Characterization of gene signatures

The core residency and circulating gene list was collected from the research of Milner and colleagues (36). Signatures across the tissues and vaccination groups were evaluated using UCell (37). The raw data underpinning the heatmap in **Fig. 5G** was displayed in Supplementary Table S2.

Construction of T_{RM}-cell regulatory network

To better understand and explore the upstream regulatory events affecting T_{RM}-cell formation, we constructed the regulatory network of T_{RM} cells. The network was built in two steps. The first was to identify the transcription factors (TF) that regulated the formation of T_{RM} cells in lung tissue. Cell trajectory and pseudo-time inference for the Naïve-Central Memory-Cytotoxic transition of the $CD8^+$ T cells were performed using Monocle 3 (38). Graph_test function in Monocle was used to evaluate trajectory genes, entries with morans_I >0.1 and q value <0.01 were considered as significant. The TFs in trajectory genes were identified using the mouse transcription factor catalog downloaded from SCENIC v1.3.1 (39). We also refined the candidate TF list using differential expression analysis between vaccination groups in the lung (day 2 vs. naïve for single i.n. and day 2 vs. day 0 for i.n. boost, respectively). Volcano plots of differential genes were generated using EnhancedVolcano v1.12.0 R package (https://github.com/kevinblighe/EnhancedVolcano). Further, we used pySCENIC (39) to assess the target gene regulatory activity of the filtered TFs and built a regulatory network based on the TF-core residency gene pairs using Cytoscape v3.9.1 (RRID: SCR_003032; ref. 40). Enriched gene ontology (GO) pathways of prioritized TF target genes were assessed using R package clusterProfiler v4.2.2 (RRID: SCR_016884; ref. 41). The second step was to evaluate the potential regulatory impact of tissue cells in the lung on the prioritized T_{RM}-associated TFs. Lung tissue cell to $CD8^+$ T-cell communication was inferred using NicheNet (R package NicheNet v1.1.1; ref. 42). The parameters in the NicheNet analysis process were set to (i) log-fold change cutoff of 0.25, (ii) top 250 targets for calculating ligand activities, and (iii) the default value of prioritizing weights. We filtered and retained the regulatory relationships between the top 50 ligand signals to downstream $CD8^+$ T-cell receptors and the prioritized T_{RM} -associated TFs.

Statistical analysis

Statistical analysis was performed using GraphPad Prism 8.0. Grouped analysis was generated by two-way ANOVA. Unpaired Student t tests were used to compare group means between two groups only. All error bars indicate SEM. A P value <0.05 was considered significant. n.s., $P > 0.05$; *, $P < 0.05$; **, $P < 0.01$; ***, $P < 0.001$; ****, $P < 0.0001$. The number of animals in each group and the specific details of statistical tests are reported in the figure legends.

Data availability

Raw and processed scRNA-seq data have been deposited in Gene Expression Omnibus under the accession number GSE238223. All other raw data are available upon request from the corresponding authors.

Results

Systemic prime-intranasal boost immunization elicited potent polyfunctional lung T_{RM} cells

In our previous study, DNA vaccine expressing HIV-1 Gag Mosaic immunogen (DNA-Gag) could induce $CD8^+$ T-cell response against subcutaneous mesothelioma challenge (21). Meanwhile, HIV-1 Gag MHC class I tetramer (AMQMLKETI, termed AI9) is available for analyzing antigen-specific $CD8^+$ T cells (21). We, therefore, were able to use the Gag protein as a model antigen for T-cell immunity and cancer research (10, 11, 21). Here, we constructed two LAIV vaccines expressing the same Gag Mosaic based on A/CA/04/2009 (H1N1) and A/Hong Kong/1/68 (H3N2) backbones (LAIV-CA04-Gag and LAIV-HK68-Gag, respectively; Supplementary Fig. S1A–S1C). As the systemic DNA prime and intranasal LAIV boost regimen elicited high frequencies of both systemic and mucosal T–cell responses (9), we tested the DNA-Gag (i.m./EP) prime followed by LAIV-HK68-Gag (i.n.) boost (V1) immunization regimen (**Fig. 1A**). The administration route and prime-boost combination are pivotal in influencing immune responses (9, 43). We, therefore, comprehensively compared the V1 with other vaccination regimens (**Fig. 1A** and **B**). Consistent with our previous finding, the V1 regimen induced potent mucosal and systemic Gag-specific memory T–cell responses simultaneously (Supplementary Figs. S2A–S2D and S3A–S3D). Critically, the majority of responding T cells was polyfunctional with double or triple cytokine production, which was significantly stronger than other immunization strategies.

Next, we assessed the induction and functionality of lung T_{RM} cells. Antigen-specific lung $CD8^+$ T_{RM} cells were only observed in the intranasal boosted groups (**Fig. 1C** and **D**), whereas intramuscular boosted regimens elicited T_{CIRM} cells including $CD103^-$ $CD69^-$ $CD62L^-$ $CD44^+$ $CD8^+$ T_{EM} cells and $CD62L^+$ $CD44^+$ $CD8^+$ T_{CM} cells in lungs and MLN (**Fig. 1C** and **E**). Notably, the majority of $CD8^+$ T_{RM} cells generated by V2 were specific to the immunodominant NP of the influenza vector rather than to Gag (**Fig. 1F**). The heterologous prime in V1 offered an advantage in promoting the Gag immunodominance by reducing anti-influenza vector T_{RM}-cell induction. The V3 and V4 regimens could induce neither $CD8^+$ T_{RM} cells nor potent antigen-specific $CD8^+$ T-cell responses. Therefore, in a separate experiment, we further investigated the phenotype of cytokine-secreting antigen-specific lung $CD8^+$ T cells by comparing V1, V2, V5, and V6 (**Fig. 1G**). Most cytokine-secreting, antigen-specific lung $CD8^+$ T cells were identified as T_{RM} cells, indicating their potential in antigen-specific recall responses (**Fig. 1G**). These data suggested that only heterologous systemic prime-intranasal boost immunization generated robust polyfunctional antigen-specific lung $CD8^+$ T_{RM} cells.

Vaccine-elicited lung $CD8^+$ T_{RM} cells, rather than T_{CIRM} cells, mediated protective immunity against tumor lung metastasis

We next sought to evaluate the V1 regimen-elicited long-term immunity against lung metastasis (**Fig. 2A**). We found that only V1 significantly inhibited melanoma lung metastasis (**Fig. 2B–D**). Moreover, in another experiment we found that only V1 significantly inhibited metastatic mesothelioma growth in lungs (Supplementary Fig. S4A–S4C). Both models collectively demonstrated that DNA vaccine i.m./EP prime followed by LAIV i.n. boost regimen could effectively prevent tumor lung metastasis. Cancer progression is associated with immunosuppressive tumor microenvironment establishment. Soluble mediators secreting from the polymorphonuclear myeloid-derived suppressor cells (PMN-MDSC), mononuclear myeloid-derived suppressor cells (M-MDSC), and regulatory T (Treg) cells induce T-cell dysfunction and exhaustion (44). We subsequently measured the expression of exhaustion maker PD-1 on $CD8^+$ T cells and frequencies of Treg cells ($CD4^+$ $CD25^+$ $Foxp3^+$), PMN-MDSCs ($CD11b^+$ $Ly6G^+$), and M-MDSCs ($CD11b^+$ $Ly6C^+$) in lungs at the endpoint of melanoma challenge (**Fig. 2E**). Significantly lower levels of PD-1 expression on $CD8^+$ T cells and PMN-MDSC were observed in V1 group. The frequencies of natural killer (NK) cells in V1 were significantly higher than V6 but similar to V2 and V5, indicating that NK cells were unlikely the major player in reducing lung metastasis. The cytokine expression levels in V1 were significantly higher, confirming that our DNA/LAIV vaccination regimen effectively prevented the tumor-specific $CD8^+$ T-cell exhaustion and maintained the cytotoxic function (**Fig. 2E**). We further investigated the correlation between vaccine-elicited immunity and melanoma rejection. $CD4^+$ or $CD8^+$ T cells were transiently depleted in V1-vaccinated mice 1 month post the booster vaccination, and the melanoma challenge was performed 1 month post T-cell depletion (**Fig. 2F**). This approach depleted vaccine-induced antigen-specific T cells and allowed antigen nonspecific T cells to repopulate before tumor challenge, thus efficiently distinguishing the antitumor effect between these T cells (25). We first confirmed the successful T-cell depletion in blood samples (Supplementary Fig. S4D and S4E). At the time of tumor challenge, vaccine-induced antigen-specific T cells in lungs were effectively eliminated by a single injection of T cell–depleting antibodies. $CD4^+$ T-cell depletion did not affect antigen-specific $CD8^+$ T-cell functioning, vice versa (Supplementary Fig. S4F). Depletion of $CD8^+$ T cells alone impaired the vaccine-mediated protection significantly, resulting in an increasing tumor growth rate compared with V1 ($P = 0.0352$), while depletion of $CD4^+$ T cells alone did not significantly impair the tumor-protecting efficacy ($P = 0.4754$; **Fig. 2G**). Meanwhile, nonspecific T-cell activation was unlikely affected by the T-cell depletion strategy (Supplementary Fig. S5A and S5B). Collectively, the V1-induced antigen-specific $CD8^+$ T cells inhibited melanoma lung metastasis and reduced PMN-MDSC-mediated immunosuppression.

Although the frequency of $CD8^+$ T_{RM} cells is associated with better clinical outcomes in patients with lung cancer (45), T_{CIRM} cells have been considered sufficient to prevent melanoma lung metastasis (13). The interplay between vaccine-elicited T_{CIRM} and T_{RM} cells in lung metastasis protection has not been well investigated (10). To functionally distinguish vaccine-elicited T_{RM} cells from T_{CIRM} cells, we employed a parabiosis surgery with parabiont pairs sharing T_{CIRM} cells, but only the vaccinated animals retained T_{RM} cells (25). Mice were vaccinated with V1 30 days before the surgical parabiosis with naïve mice. After T_{CIRM} cells equilibrated between two parabionts, mice were separated and proceeded to the tumor challenge (**Fig. 3A** and **B**). Vaccinated parabionts reduced the tumor growth significantly

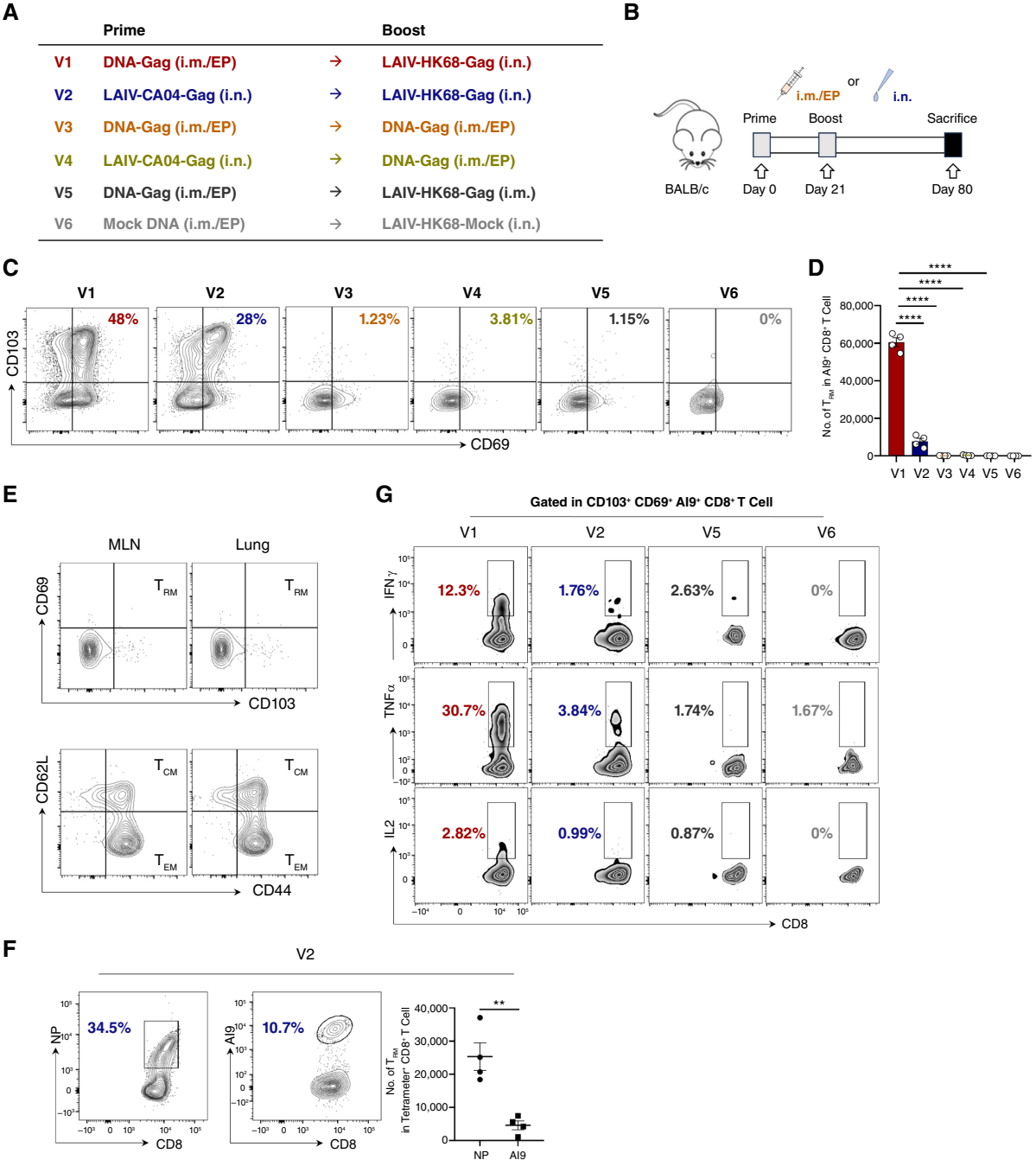

Figure 1.

Systematic prime-nasal booster immunization elicited potent polyfunctional lung T_{RM} cells. **A,** Vaccination schemes. **B,** Groups of BALB/c mice ($n = 4$) were vaccinated with different regimens. Tissues were subjected to ICS or phenotype analysis. **C,** Representative density plots were gated in AI9$^+$ CD8$^+$ T cells and CD69$^+$ CD103$^+$ CD8$^+$ T cells represented lung CD8$^+$ T_{RM} cells. **D,** Quantified lung CD8$^+$ T_{RM} cells. **E,** AI9$^+$ CD8$^+$ T-cell composition from V3 group at day 60 post booster immunization. **F,** Quantified NP$^+$ and AI9$^+$ CD8$^+$ T cells in the lungs from V2 group. **G,** Lung cells isolated from designated groups at day 60 post booster immunization were subjected to ICS. Statistics were generated by the two-tailed Student *t* test. ****, $P < 0.0001$.

compared with naïve parabionts (**Fig. 3C–E**). Of note, at the earliest time that tumor growth was measured, the tumor inhibition effect was only observed in vaccinated parabionts (**Fig. 3F**). Therefore, T_{RM} cells provided frontline surveillance and immediate tumor elimination function, and the delayed T_{CIRM}-cell functioning resulted in a minor tumor-clearing effect. Collectively, V1 regimen served as an effective strategy to elicit CD8$^+$ T_{RM} cells against lung tumor metastasis, and vaccine-induced lung CD8$^+$ T_{RM} cells were pivotal in the protection compared to the T_{CIRM} cells.

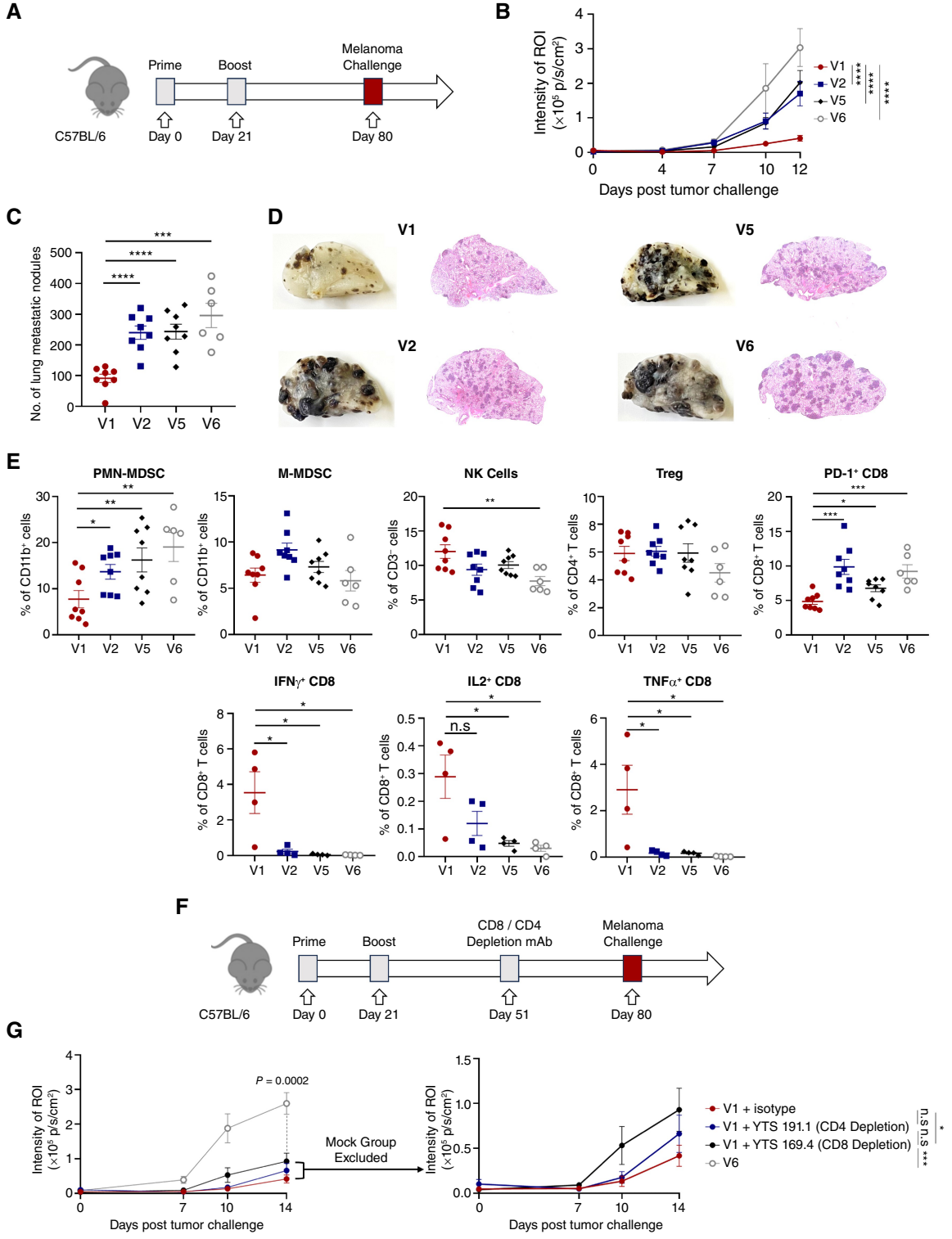

Figure 2.

Systematic prime-nasal booster immunization enhanced protection against melanoma lung metastasis. **A,** Mice that received V1, V2, V5, or V6 vaccine regimens ($n = 8$ for V1, V2, and V5 group; $n = 6$ for V6 group) were challenged by B16-Gag cells at day 60 post boost vaccination. **B,** The tumor growth rate. **C** and **D,** At the endpoint (day 12 post boost vaccination), half of the lungs were fixed with Fekete's fixative solution to quantify the lung metastasis nodules (**C**) and hematoxylin and eosin (**D**) staining. **E,** PMN-MDSC, M-MDSC, NK cells, Treg, PD-1+, and Gag-specific CD8+ T cells were quantified from the other half of the lungs. **F,** Experiment schedule. **G,** The tumor growth rate and bioluminescence intensity. Two-way ANOVA was applied for **B** and **G**. Two-tailed Student *t* tests were applied for **C** and **E**. *, $P < 0.05$; **, $P < 0.01$; ***, $P < 0.001$; ****, $P < 0.0001$.

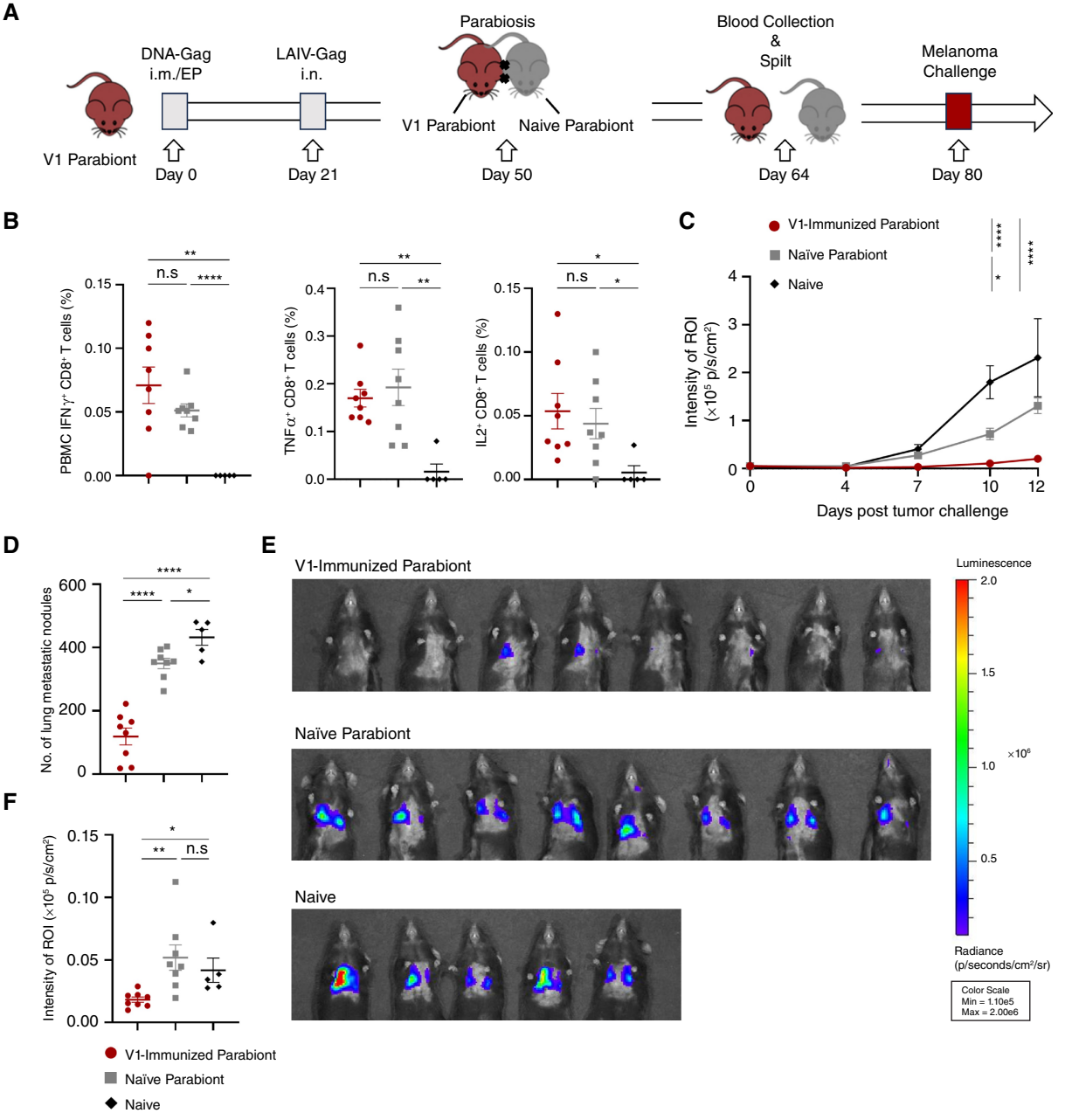

Figure 3.

Vaccine-elicited CD8$^+$ T_{RM} cells protected melanoma lung metastasis. **A,** Experiment schedule. **B,** Quantified Gag-specific CD8$^+$ T cells were measured in PBMC collected from parabiont pairs by ICS. Five naïve mice were included as the control. **C,** Tumor growth rate. **D** and **E,** Quantified results at the endpoint (day 12 post-tumor inoculation). **F,** Early melanoma progression was measured at day 4 post-tumor challenge. Two-tailed Student *t* tests were applied for **B**, **D**, and **F**. Two-way ANOVA was applied for **C**. n.s., nonsignificant; *, $P < 0.05$; **, $P < 0.01$; ****, $P < 0.0001$.

T_{CM} cells elicited by systemic prime vaccination were the major precursors of boost immunization-induced lung T_{RM} cells

Mucosal boost vaccination or chemokine has been used to amplify local T-cell response for enhanced protection (46). We showed that the V1 prime-boost vaccination generated more T_{RM} cells than the intranasal vaccination alone (**Fig. 4A**). Systemic immunization alone elicited large numbers of T_{EM} and T_{CM} cells but not T_{RM} cells in the lungs, MLN, and spleen (**Fig. 1E**). These results indicated that DNA prime-generated T_{CM} or T_{EM} cells might serve as lung T_{RM}-cell precursors and their differentiation was triggered by intranasal booster immunization. We, therefore, adoptively transferred the same number of CD45.2$^+$ OVA-specific CD8$^+$ T_{EM} or T_{CM} cells into CD45.1 recipients to

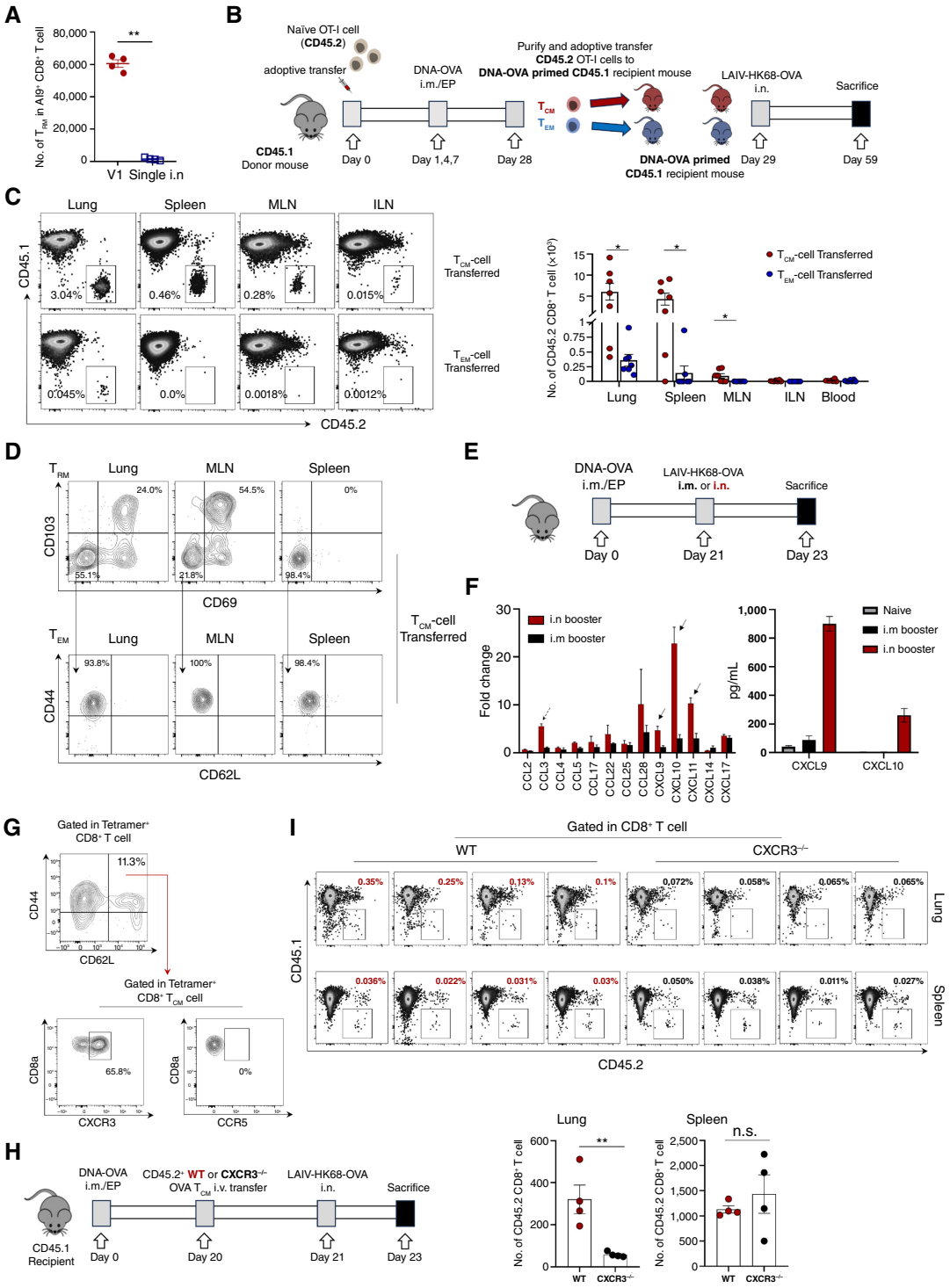

Figure 4.

Systemic primed T_{CM} cells were the major precursors of lung T_{RM} cells. **A,** Mice received either DNA/LAIV prime-boost vaccination (red) or single LAIV i.n. vaccination (blue; $n = 4$). Lung AI9$^+$ CD8$^+$ T_{RM} cells were quantified at 30 days post LAIV-HK68-Gag immunization. **B,** Experiment schedule. **C,** Quantified transferred T_{CM} and T_{EM} cells in various organs. **D,** Phenotype analysis of transferred T_{CM} cells. Density plots were gated on CD45.2$^+$ CD8$^+$ T cells. **E,** Experiment schedule. At day 2 post boost vaccination, half of the lungs were homogenized for chemokine mRNA and protein detection. The other half of the lungs proceeded to measure the chemokine receptor. **F,** The mRNA and protein level of chemokines in lungs. Significant differences were observed in the arrow-indicated chemokines. **G,** CCR5 and CXCR3 expression on CD8$^+$ T_{CM} cells in the lungs from intranasally boosted mice. **H,** Experiment design. **I,** Transferred wild-type or CXCR3$^{-/-}$ CD8$^+$ T_{CM} cells were quantified from recipients at day 2 post-adoptive transfer. Two-tailed Student *t* tests were applied. n.s., nonsignificant; *, $P < 0.05$; **, $P < 0.01$.

investigate their differentiation capacity, respectively (**Fig. 4B**; refs. 17, 18). After booster vaccination, transferred $CD8^+$ T_{CM} cells were retained for a prolonged period in the lung, MLN, and spleen over the memory phase. In contrast, few transferred T_{EM} cells could be observed in different tissues (**Fig. 4C**). Boosted T_{CM} cells illustrated the phenotype of T_{EM} and T_{RM} cells in MLN and lung at the memory phase (**Fig. 4D**). Consistent with the previous findings in other organs and mucosa, T_{CM} cells retained stemness to repopulate into heterosubtypic memory T cells (47) but T_{EM} cells show less proliferative capacity upon restimulation (1, 2).

T-cell differentiation is initiated by early trafficking and accumulation in the secondary lymphoid organ or infected tissue, a process largely dependent on chemokine and receptor interaction (48, 49). To evaluate whether these interactions could mediate early T_{CM}-cell lung trafficking, groups of mice received different booster vaccinations (**Fig. 4E**). Day 2 post-infection was previously reported as the earliest time point that T-cell recruitment was observed in lung (48). Increased mRNA levels of CCR5 ligand (CCL3) and CXCR3 ligands (CXCL9, CXCL10, and CXCL11) were observed in lungs from i.n. boosted mice compared with i.m. boosted group (**Fig. 4F**). Increased CXCL9 and CXCL10 protein levels were also detected. However, CXCR3 but not CCR5 was highly expressed on $CD8^+$ T_{CM} cells (**Fig. 4G**). We further introduced wild-type (WT) or CXCR3 knockout ($CXCR3^{-/-}$) T_{CM} cells to verify the function of CXCR3 ligand–receptor interaction in mediating $CD8^+$ T_{CM}-cell infiltration (**Fig. 4H**). Compared with the $CXCR3^{-/-}$ T_{CM} cells, increasing WT OVA $CD8^+$ T_{CM} cells were recruited into the lung after the i.n. vaccination. However, no significant difference was observed in the spleen (**Fig. 4I**). Previous research has presented controversial perspectives on whether CXCR3 chemotaxis mediates T-cell lung recruitment at later time points.(49, 50) In our results, no significant difference was observed at day 14 post i.n. immunization (Supplementary Fig. S6A and S6B). Therefore, CXCR3 receptor–ligand interactions promoted antigen-specific T_{CM}-cell early recruitment into the lungs after the intranasal booster immunization, which might contribute to the subsequent T_{RM}-cell differentiation.

Intranasal booster vaccination conferred T_{RM} cell features to lung cytotoxic T cells upon activation

To better understand the $CD8^+$ T_{CM}- to T_{RM}-cell differentiation process in the systemic prime-mucosal boost vaccination regimen, total cells from lungs, MLN, and spleen were extracted from mice immunized with the DNA-OVA i.m./EP plus LAIV-HK68-OVA i.n. regimen at 21 days post-DNA-OVA prime immunization (day 0), 2, 4, and 30 days post LAIV-HK68-OVA booster vaccination for scRNA-seq. The rationality for sampling time points was based on the T_{CM}-cell reactivation (Supplementary Fig. S7A) and early recruitment (48) that were detectable as early as day 2 post-vaccination or post-infection. Day 4 post-booster vaccination was the earliest time point that the phenotypic changes of transferred $CD8^+$ T_{CM} cells could be observed (Supplementary Fig. S7A). These two time points might cover large amounts of early transcriptional regulation events in T_{CM}- to T_{RM}-cell development. To evaluate the effect of systemic prime vaccination, samples from single intranasal vaccinated mice were also sent for sequencing at indicated time points as comparisons (**Fig. 5A**). A total of 21 distinct cell clusters were defined according to previous studies (Supplementary Fig. S7B; refs. 32–34) and visualized (**Fig. 5B**; ref. 33). To reveal the T-cell function and differentiation dynamic, $CD8^+$ T cells were further classified into four populations (**Fig. 5C**). Naïve $CD8^+$ T cells expressed *LEF1*, *CCR7*, *TCF7*, *SELL* (51). Central memory $CD8^+$ T cells exhibited a similar *CCR7*, *TCF7*, *SELL* expression as naïve T cells but with additional expression of *LY6C2*, *CD44*, *IL2RB* (52–54). Cytotoxic $CD8^+$ T cells displayed enhanced expression of *CCL5*, *GZMB*, *NKG7*, *PRF1* (55, 56). *TOP2A*, *STMN1*, *MKI67* (55) were highly expressed in cycling $CD8^+$ T cells (**Fig. 5D**).

Increasing frequencies of cytotoxic $CD8^+$ T cells were observed in lungs and spleens harvested from prime-boost immunized mice at day 30 post-final vaccination (memory phase; **Fig. 5E**). It was consistent with our previous observation that the DNA/LAIV regimen provided better protection against lung metastasis (**Fig. 2**; Supplementary Fig. S4). Instead of identifying a unique lung $CD8^+$ T_{RM}-cell population in the UMAP (**Fig. 5F**), the core tissue-residency signature gene expression was significantly enriched in the lung cytotoxic T cells at different time points after the booster vaccination (**Fig. 5G** and **H**; ref. 36). Different from the FACS analysis, *CD69* and *ITGAE* (CD103 gene) were insufficient for accurately characterizing lung $CD8^+$ T_{RM} cells (**Fig. 5C**). Previous research utilized a set of signature genes to characterize $CD8^+$ T_{RM} cells (36). Compared with other $CD8^+$ T cell subclusters, the core residency genes were significantly enriched in the lung cytotoxic $CD8^+$ T cells (**Fig. 5C**), and this provided the rationale for us to further investigate the T_{RM} cell differentiation in the cytotoxic subcluster. On the contrary, the expression level of core circulating gene signatures in cytotoxic T cells was similar in lungs and spleens (Supplementary Fig. S8A and S8B; ref. 36). Compared with lungs harvested from the naïve and DNA i.m./EP primed mice, the upregulation of core residency genes had already been observed as early as day 2 post booster vaccination. It suggested that most immunoregulatory events might occur directly in the lung after i.n. booster immunization. We, therefore, further developed a detailed GO pathway enrichment analysis to describe the kinetic changes of different cell subpopulations (Supplementary Fig. S9A and S9B). Compared with the single i.n. vaccination, the i.n. booster vaccination induced more regulatory activities in the $CD8^+$ T cell subclusters at different time points. It is worth mentioning that the MLN DC subclusters in the booster-immunized group illustrated more regulations of immune responses and cell–cell interactions especially in early time points post-immunization. In conclusion, compared to the single i.n. immunization, prime-boost immunization induced more immunoregulatory events and a stronger immune response in both lungs and spleen early after vaccination. Additionally, compared with spleen and MLN, the core residential genes were significantly enriched in the lung across different time points post intranasal vaccination (**Fig. 5H**). Meanwhile, compared with the single i.n. vaccination, the core residency genes were significantly enriched in the prime-boost immunization group at different time points (**Fig. 5H**). Therefore, the booster vaccination in the systemic prime-mucosal boost regimen endowed lung cytotoxic $CD8^+$ T cells with T_{RM}-cell properties at the early activation stage, and the residency characteristics were maintained into the memory phase.

The differentiation fate of T_{CM} to lung T_{RM} cells was determined at the reactivation stage after the intranasal booster vaccination

Previous research has identified several key molecular determinants and depicted early transcriptional profiling of T_{RM}-cell

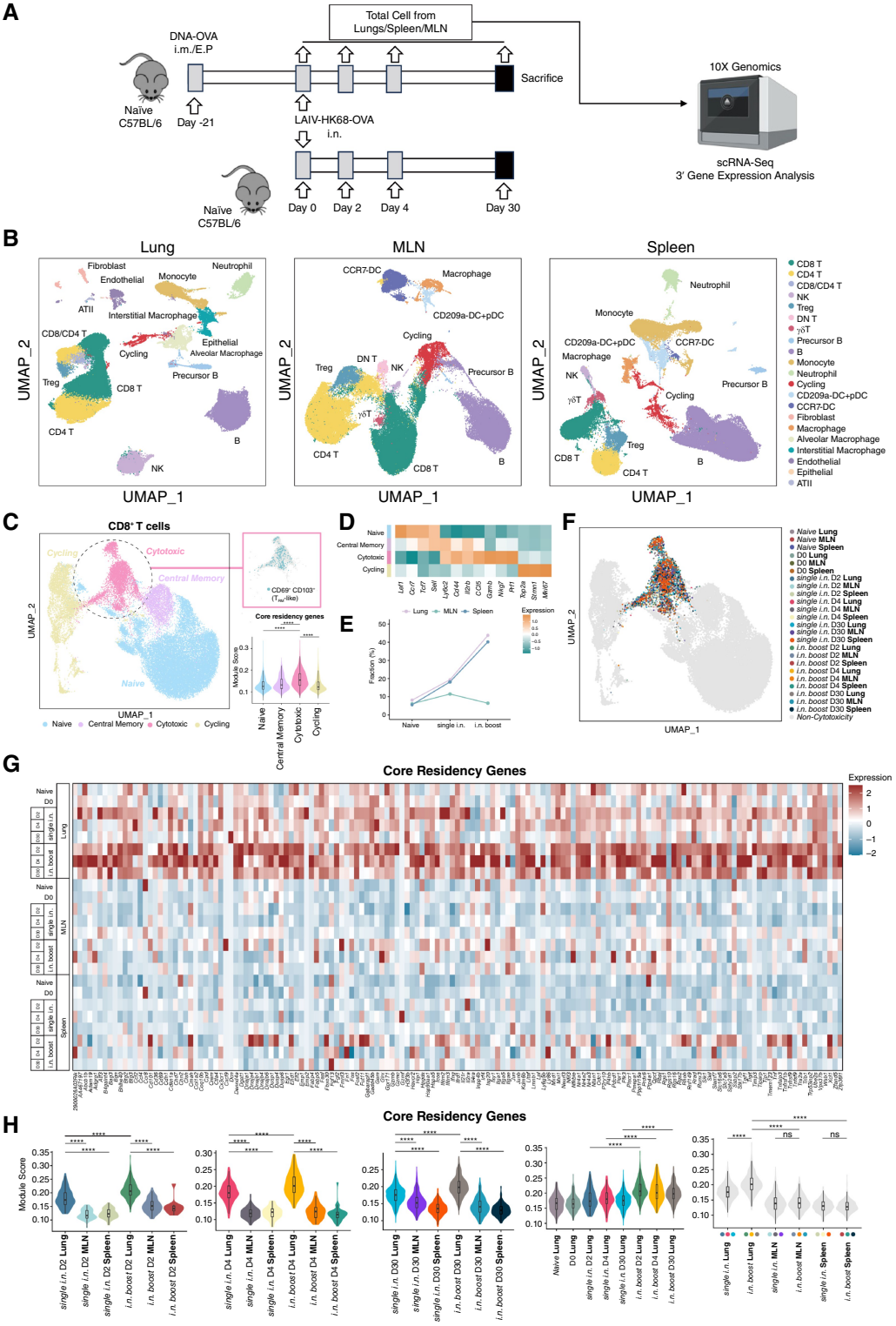

Figure 5.

Intranasal booster vaccination conferred T_{RM} features to lung cytotoxic T cells upon activation. **A,** Study design ($n = 3$). **B,** UMAP visualization of 21 cell populations and **C** $CD8^+$ T cells in different tissues. **D,** Signature gene expression in each $CD8^+$ T-cell subset. **E,** The comparison of cytotoxic $CD8^+$ T-cell frequency in different tissues among different vaccinated groups at day 30 post-final vaccination. **F,** The distribution of cytotoxic T cells in each sample. **G,** Core tissue–residency gene expression across tissues and vaccination groups. **H,** From left to right, gene module score of core residency genes in $CD8^+$ T cells in different tissues at day 2, day 4, day 30 post i.n. vaccination; comparison across lung samples from different time points; considered samples from three time points of each tissue as an entirety. ns, nonsignificant; ****, $P < 0.0001$.

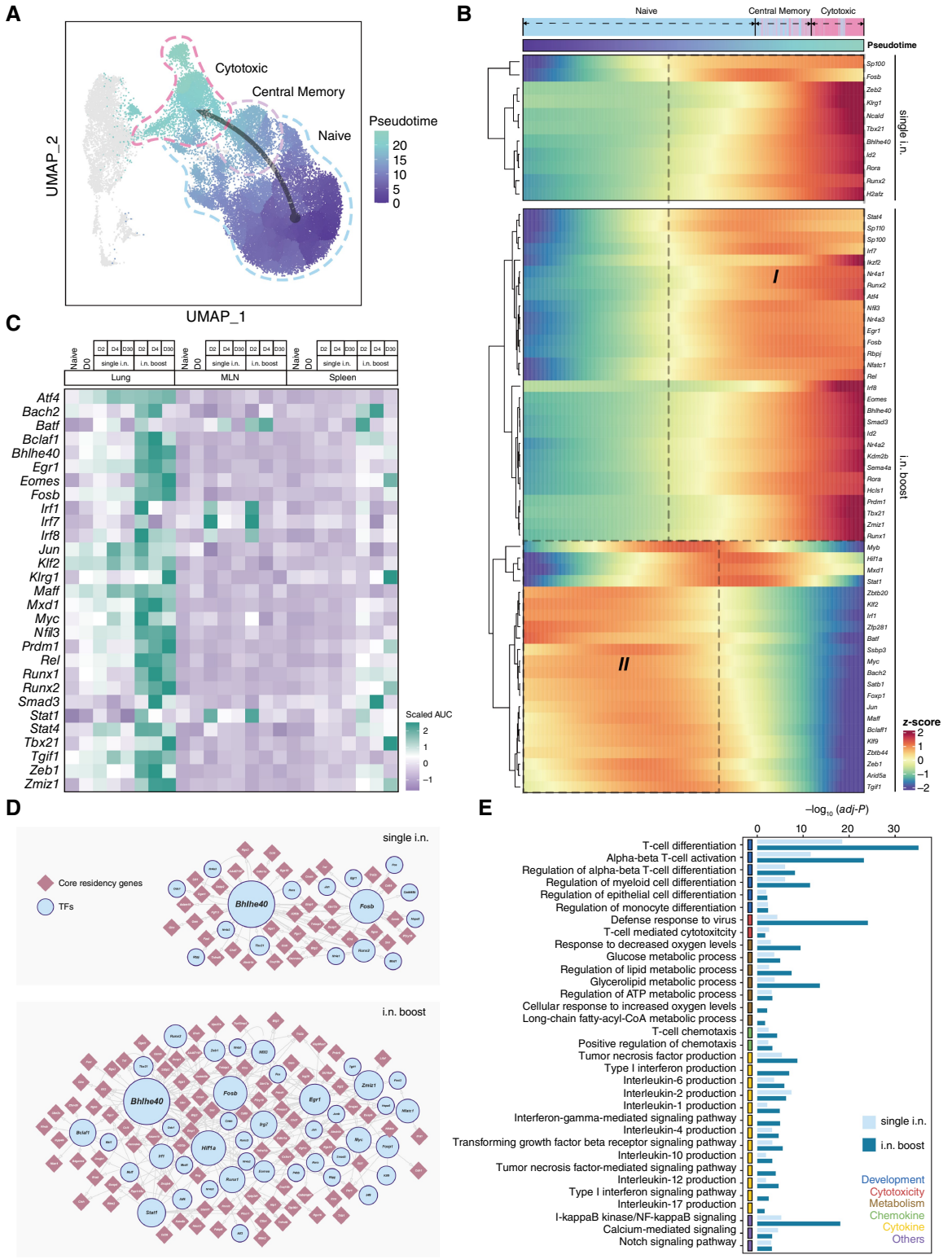

Figure 6.

Trajectory TFs regulated T_{RM}-cell differentiation at early reactivation phase. **A,** UMAP representation of naïve-T_{CM} cytotoxic cell transition process colored by pseudotime. **B,** Heatmap representing the transcriptomic progress of trajectory TFs through the transition process. **C,** Heatmap of scaled AUC scores of TFs across tissues and vaccination groups, as estimated using SCENIC. **D,** Prioritized TF core residency gene network in single i.n. group and i.n. boosted group. The size of TF dots represented the relative number of coresidency genes regulated by the designated TF. **E,** Enriched GO pathways of prioritized TF target genes mentioned in **D**.

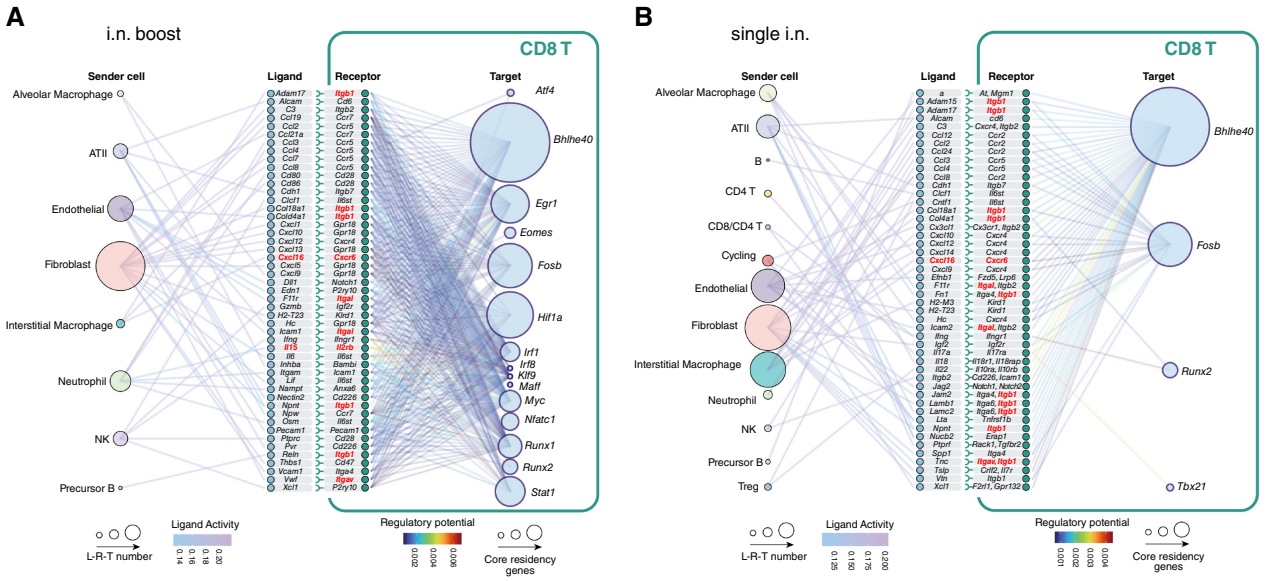

Figure 7.

Intercellular communication between cells within the lung and the CD8+ T cells instructed the T_{RM}-associated transcriptional program. Regulatory network of tissue cells prioritized T_{RM} cell–associated TFs in the lung harvested from day 2 post i.n. boosted group (**A**) and single i.n. group (**B**). T_{RM} cell–related cellular interactions are highlighted in red. The dot size for the sender cell reflects the number of ligand–receptor target pairs involved. The dot size for the target gene reflects the number of regulated core residency genes.

development in the effector phase (from day 4 to 12 post-infection; refs. 23, 56). In our results, however, the T_{RM} feature had already been enriched in lung CD8+ T cells at the early reactivation stage (day 2 post i.n. booster vaccination; **Fig. 5G**) when the T-cell activation marker CD69 was upregulated and the majority of antigen-specific CD8+ T_{CM} cells had not undergone phenotypic changes (Supplementary Fig. S7A). Given that the terminal fate of activated CD8+ T cells had potentially been determined in their first division (54), we hypothesized that the T_{CM}-cell to lung T_{RM}-cell differentiation had already been determined at the early reactivation stage. We performed the pseudotime analysis among different CD8+ T-cell clusters to investigate the T_{RM}-cell differentiation trajectory (**Fig. 6A**). Pseudotime suggested a developmental trajectory from naïve T cells to T_{CM} cells, and then to cytotoxic T cells. T_{CM} cell was a subset of antigen-experienced T cells compared to naïve T cells, and therefore located at an intermediate stage of differentiation. We subsequently enumerated the TFs that promoted the aïve-T_{CM}-cytotoxic cell transition. To describe the early transcriptional regulations in the lung T-cell differentiation and distinguish the alteration induced by the single i.n. from the prime-boost vaccination, we listed the upregulated trajectory TFs in lungs harvested at day 2 post i.n. boost and single i.n. vaccination. Lungs collected from the i.m./EP primed (day 0 sample) and naïve mice were set as the filter baseline, respectively (Supplementary Fig. S10A and S10B). We defined 2 TF clusters based on the dynamic expression pattern of TFs along the pseudotime differentiation. The cluster I TFs regulated the terminal differentiation fate towards cytotoxic T cells, while the cluster II TFs mainly regulated the differentiation process toward T_{CM} cells (**Fig. 6B**). TFs that had previously been shown to regulate CD8+ T_{RM}-cell development (*NR4A1*, *NR4A2*, *NR4A3*, *BHLHE40*, *PRDM1*, *SMAD3*, *ID2*, *EGR1*, *REL*, *IKZF2*; refs. 23, 56, 57) had already been highly enriched in T_{CM} cells at day 2 post i.n. vaccination. Meanwhile, more TFs controlling tissue residency were found in lungs from the prime-boost group, indicating that prime-boost vaccination enriched more T_{RM}-cell developmental regulatory activities.

TFs in **Fig. 6B** with high regulatory activity were then compared among different samples (**Fig. 6C**). TFs actively regulating lung CD8+ T-cell differentiation at the early reactivation stage were found specifically enriched in lungs from the prime-boost vaccinated group. We further established the regulatory network to investigate the regulatory relationship between active TFs (**Fig. 6C**) and residency genes (**Fig. 5G**). Many high-activity TFs exhibited an enriched residency gene regulation (**Fig. 6D**), including previously reported T_{RM} cell core regulatory TFs (*BHLHE40*, *EGR1*, *PRDM1*, *FOSB*, *EOMES*, *IRF1*, *IRF7*, *IRF8*, *STAT1*, *TGIF1*, *TBX21*; refs. 56, 58–60; bioRxiv 2022.05.04.490680). Some TFs were previously reported to regulate the residency of other immune cells but not T_{RM} cells (*NFIL3*, *RUNX1*, *RUNX2*; refs. 61–63). In addition, TFs participated in the regulation of tissue residency by potentially targeting other residency-related TFs (*RUNX3*, *STAT4*, *NR4A1-3*, *FOSL2*, *IRF4*, *JUN*, *JUNb*; refs. 36, 56). GO enrichment analysis of gene regulatory network in **Fig. 6D** suggested that multiple pathways related to the CD8+ T_{RM}-cell induction and maintenance were significantly upregulated in the prime-boost vaccinated group (**Fig. 6E**), including TGFβ signaling (56, 64), lipid metabolism (65), and IKK2/NFκB signaling (56). These data collectively suggested that the terminal T_{RM}-cell differentiation fate of a portion of CD8+ T_{CM} cells had very likely been determined at the early reactivation stage.

Intercellular communication instructed the early transcriptional program in T_{RM}-cell development

To further understand the lung tissue microenvironment that instructed the T_{CM}- to T_{RM}-cell differentiation, we inferred the potential regulation between cells within the lung and $CD8^+$ T cells. Several ligand–receptor interactions were enhanced in the lung at day 2 post the i.n. vaccination (Supplementary Fig. S11A and S11B). Subsequently, we established a potential regulatory network between the residency-associate TFs (**Fig. 6C**) and the high-activity ligand–receptor interactions (**Fig. 7**). Based on previous research, several ligand–receptor pairs were identified as influencing T_{RM}-cell development and function. For instance, the IL15-CD122 (*IL2RB*) interaction affects the initial $CD8^+$ T_{RM} cell lodgment (64) and subsequent maintenance in tissues (66). CXCR6 mediates the localization of $CD8^+$ T_{RM} cells in the airways (67). The Notch signaling pathway is suggested to play a role in $CD8^+$ T_{RM}-cell development and boosting lung cancer T-cell response (68). The cytotoxicity of CCR5-deficient memory $CD8^+$ T cells is significantly impaired in the airway (48). These receptors on $CD8^+$ T cells predominantly received signals from endothelial cells, fibroblasts, interstitial macrophages, and neutrophils, subsequently triggering the regulation of downstream residency-associated TFs (**Fig. 7A**; Supplementary Tables S3 and S4). Fewer T_{RM}-associated regulatory events were identified in the lungs at day 2 post single i.n. immunization (**Fig. 7B**), consistent with the lower $CD8^+$ T_{RM} cells generated after the single i.n. vaccination (**Fig. 4A**). Our unbiased analysis established a potential regulatory network connecting these intercellular communications with the downstream transcriptional program of $CD8^+$ T_{RM}-cell early differentiation.

Discussion

Functional lung $CD8^+$ T_{RM} cells have been proven to be pivotal in protection against viral infection and cancer progression in both animal and human studies (46, 69). Several intranasal vaccination strategies can induce lung $CD8^+$ T_{RM} cells, providing partial protection against tumor lung metastasis. These studies, however, did not differentiate explicitly the role of vaccine-induced lung $CD8^+$ T_{RM} cells and T_{CIRM} cells against tumor lung metastasis (10, 11). In this study, we investigated a heterologous DNA vaccine i.m./EP prime and LAIV-based vaccine i.n. boost regimen for inducing robust lung $CD8^+$ T_{RM}-cell responses, which achieved protection against melanoma and mesothelioma lung metastasis significantly. Using the parabiosis model, we demonstrated that the regimen-induced lung $CD8^+$ T_{RM} cells rather than T_{CIRM} cells played a central role in protection against tumor lung metastasis.

The underlying mechanism of lung $CD8^+$ T_{RM}-cell induction in heterologous systemic prime-intranasal boost vaccination remains poorly understood. We demonstrated that T_{CM} cells generated by systemic DNA prime served as the major precursors of lung $CD8^+$ T_{RM} cells. Intranasal LAIV boost immunization then created a local chemokine milieu to recruit T_{CM} cells into the lung in a CXCR3-dependent manner, which further enhanced the pool of T_{RM} cells for long-term protection. Subsequent scRNA-seq analysis also demonstrated that the intranasal boost vaccination triggered the T_{CM}-cell to T_{RM}-cell differentiation at the reactivation stage. These findings appear to be discrepant with previous studies, showing that T_{EM} cells source the lung $CD8^+$ T_{RM}-cell population (18, 19). It is possible that the discrepancy is due to distinct stages engaged for T_{RM}-cell induction. For example, Slütter performed the adoptive transfer 21 days post-influenza pulmonary infection (20). As the influenza virus in infected lung is typically cleared within 15 days (70), there is no persistent antigen presentation process to reactivate recruited memory T cells, but T_{EM} cells can be recruited by local inflammation and converted to T_{RM} cells later (19, 20). In this study, the adoptive transfer of T_{CM} and T_{EM} cells was set at 1 day before the intranasal immunization (**Fig. 4B**). T_{CM} cells rather than T_{EM} cells could effectively differentiate into lung T_{RM} cells after the cognate antigen reactivation, which was consistent with previous studies on skin T_{RM} cell induction (15–17). Therefore, T_{CM} cells gave rise to the T_{RM}-cell population during the reactivation stage, and subsequent vaccine-induced lung inflammatory environment might recruit T_{EM} cells to replenish T_{RM} cells (18–20).

Previous studies described the earliest transcriptional profile of early precursors in the naïve T-cell to T_{RM}-cell differentiation since day 4 post-infection (56, 71). We, however, advanced the detection of T_{CM}-cell reactivation in different tissues as early as day 2 post the i.n. immunization. T_{CM} cells had already undergone the phenotype switch at day 4 (Supplementary Fig. S7A). It is consistent with previous reports that memory T cells always progress more swiftly than the naïve T-cell population (72). Our findings described the early transcriptional regulatory events on the total T_{CM} cells, which covered antigen-specific T_{CM} cells. Future studies can apply cell barcode techniques to precisely describe vaccine-induced memory T cells at higher resolution.

Despite some mechanisms underlying the T_{RM}-cell development have previously been revealed (73, 74), the connections between intercellular and intracellular regulations remain poorly understood. Here, we indicated the regulatory potential of cells within the lungs to modulate $CD8^+$ T_{RM} development. We, therefore, bridged the link between intercellular communication and cell-intrinsic T_{CM}- to T_{RM}-cell regulatory events. Overall, our work demonstrated a mechanism underlying the lung $CD8^+$ T_{RM}-cell induction by the systemic prime-mucosal boost immunization regimen and provided a better understanding for future optimization of vaccine strategies.

Authors' Disclosures

Z. Chen reports grants from Research Grants Council Theme-Based Research Scheme, Collaborative Research Fund, Research Grants Council General Research Fund, Health@InnoHK, Innovation and Technology Commission, Emergency Key Program of Guangzhou Laboratory, Wellcome Trust, and Donations from the Friends of Hope Education Fund during the conduct of the study. No disclosures were reported by the other authors.

Authors' Contributions

H. Xu: Conceptualization, data curation, software, formal analysis, methodology, writing–original draft. **M. Yue:** Software, formal analysis, methodology. **R. Zhou:** Methodology. **P. Wang:** Methodology. **M.Y.-C. Wong:** Methodology. **J. Wang:** Methodology. **H. Huang:** Methodology. **B. Chen:** Methodology. **Y. Mo:** Methodology. **R.C.-Y. Tam:** Methodology. **B. Zhou:** Methodology. **Z. Du:** Methodology. **H. Huang:** Methodology. **L. Liu:** Methodology. **Z. Tan:** Methodology. **K.-Y. Yuen:** Resources, project administration. **Y. Song:** Resources, project administration. **H. Chen:** Resources, project administration. **Z. Chen:** Conceptualization, supervision, writing–original draft, writing–review and editing.

Acknowledgments

This study was supported by the Research Grants Council Theme-Based Research Scheme (T11-706/18-N, T12-703/23-N, and T11-702/24-N to Z. Chen) and Collaborative Research Fund (C7156-20G to Z. Chen), the Research Grants Council General

Research Fund (17117422), the University Development Fund and Li Ka Shing Faculty of Medicine Matching Fund from HKU to the AIDS Institute, Health@InnoHK (Center for Virology, Vaccinology and Therapeutics), the Innovation and Technology Commission, Emergency Key Program of Guangzhou Laboratory (EKPG22-01 to Z. Chen), Wellcome Trust (P86433 to Z. Chen), and Donations from the Friends of Hope Education Fund. The scRNA-seq service was provided by the Centre for PanorOmic Sciences (CPOS), HKU.

Note

Supplementary data for this article are available at Cancer Research Online (http://cancerres.aacrjournals.org/).

Received October 25, 2023; revised March 15, 2024; accepted July 16, 2024; published first July 18, 2024.

References

1. Mueller SN, Gebhardt T, Carbone FR, Heath WR. Memory T cell subsets, migration patterns, and tissue residence. Annu Rev Immunol 2013;31:137–61.
2. Sallusto F, Geginat J, Lanzavecchia A. Central memory and effector memory T cell subsets: function, generation, and maintenance. Annu Rev Immunol 2004;22:745–63.
3. Gattinoni L, Speiser DE, Lichterfeld M, Bonini C. T memory stem cells in health and disease. Nat Med 2017;23:18–27.
4. Renkema KR, Huggins MA, Borges da Silva H, Knutson TP, Henzler CM, Hamilton SE. KLRG1+ memory CD8 T cells combine properties of short-lived effectors and long-lived memory. J Immunol 2020;205:1059–69.
5. Olson JA, McDonald-Hyman C, Jameson SC, Hamilton SE. Effector-like CD8+ T cells in the memory population mediate potent protective immunity. Immunity 2013;38:1250–60.
6. Mueller SN, Mackay LK. Tissue-resident memory T cells: local specialists in immune defence. Nat Rev Immunol 2016;16:79–89.
7. Rotrosen E, Kupper TS. Assessing the generation of tissue resident memory T cells by vaccines. Nat Rev Immunol 2023;23:655–65.
8. Ku MW, Bourgine M, Authié P, Lopez J, Nemirov K, Moncoq F, et al. Intranasal vaccination with a lentiviral vector protects against SARS-CoV-2 in preclinical animal models. Cell Host Microbe 2021;29:236–49.e6.
9. Zhou R, Wang P, Wong YC, Xu H, Lau SY, Liu L, et al. Nasal prevention of SARS-CoV-2 infection by intranasal influenza-based boost vaccination in mouse models. EBioMedicine 2022;75:103762.
10. Rakhra K, Abraham W, Wang C, Moynihan KD, Li N, Donahue N, et al. Exploiting albumin as a mucosal vaccine chaperone for robust generation of lung-resident memory T cells. Sci Immunol 2021;6:eabd8003.
11. Mei Y, Zhao L, Liu Y, Gong H, Song Y, Lei L, et al. Combining DNA vaccine and AIDA-1 in attenuated Salmonella activates tumor-specific CD4+ and CD8+ T-cell responses. Cancer Immunol Res 2017;5:503–14.
12. Ganesan AP, Clarke J, Wood O, Garrido-Martin EM, Chee SJ, Mellows T, et al. Tissue-resident memory features are linked to the magnitude of cytotoxic T cell responses in human lung cancer. Nat Immunol 2017;18:940–50.
13. Molodtsov AK, Khatwani N, Vella JL, Lewis KA, Zhao Y, Han J, et al. Resident memory CD8+ T cells in regional lymph nodes mediate immunity to metastatic melanoma. Immunity 2021;54:2117–32.e7.
14. Seder RA, Hill AV. Vaccines against intracellular infections requiring cellular immunity. Nature 2000;406:793–8.
15. Fonseca R, Beura LK, Quarnstrom CF, Ghoneim HE, Fan Y, Zebley CC, et al. Developmental plasticity allows outside-in immune responses by resident memory T cells. Nat Immunol 2020;21:412–21.
16. Matos TR, Gehad A, Teague JE, Dyring-Andersen B, Benezeder T, Dowlatshahi M, et al. Central memory T cells are the most effective precursors of resident memory T cells in human skin. Sci Immunol 2022;7:eabn1889.
17. Enamorado M, Iborra S, Priego E, Cueto FJ, Quintana JA, Martínez-Cano S, et al. Enhanced anti-tumour immunity requires the interplay between resident and circulating memory CD8+ T cells. Nat Commun 2017;8:16073.
18. Slütter B, Van Braeckel-Budimir N, Abboud G, Varga SM, Salek-Ardakani S, Harty JT. Dynamics of influenza-induced lung-resident memory T cells underlie waning heterosubtypic immunity. Sci Immunol 2017;2:eaag2031.
19. Takamura S, Yagi H, Hakata Y, Motozono C, McMaster SR, Masumoto T, et al. Specific niches for lung-resident memory CD8+ T cells at the site of tissue regeneration enable CD69-independent maintenance. J Exp Med 2016;213:3057–73.
20. Takamura S, Kohlmeier JE. Establishment and maintenance of conventional and circulation-driven lung-resident memory CD8+ T cells following respiratory virus infections. Front Immunol 2019;10:733.
21. Liu W, Wong YC, Chen SMY, Tang J, Wang H, Cheung AKL, et al. DNA prime/MVTT boost regimen with HIV-1 mosaic Gag enhances the potency of antigen-specific immune responses. Vaccine 2018;36:4621–32.
22. Wang P, Zheng M, Lau SY, Chen P, Mok BW, Liu S, et al. Generation of DelNS1 influenza viruses: a strategy for optimizing live attenuated influenza vaccines. mBio 2019;10:e02180–19.
23. Kok L, Dijkgraaf FE, Urbanus J, Bresser K, Vredevoogd DW, Cardoso RF, et al. A committed tissue-resident memory T cell precursor within the circulating CD8+ effector T cell pool. J Exp Med 2020;217:e20191711.
24. Szabo PA, Miron M, Farber DL. Location, location, location: tissue resident memory T cells in mice and humans. Sci Immunol 2019;4:eaas9673.
25. Zhao J, Zhao J, Mangalam AK, Channappanavar R, Fett C, Meyerholz DK, et al. Airway memory CD4+ T cells mediate protective immunity against emerging respiratory coronaviruses. Immunity 2016;44:1379–91.
26. Zheng GX, Terry JM, Belgrader P, Ryvkin P, Bent ZW, Wilson R, et al. Massively parallel digital transcriptional profiling of single cells. Nat Commun 2017;8:14049.
27. Hao Y, Hao S, Andersen-Nissen E, Mauck WM 3rd, Zheng S, Butler A, et al. Integrated analysis of multimodal single-cell data. Cell 2021;184:3573–87.e29.
28. Young MD, Behjati S. SoupX removes ambient RNA contamination from droplet-based single-cell RNA sequencing data. Gigascience 2020;9:giaa151.
29. Wolock SL, Lopez R, Klein AM. Scrublet: computational identification of cell doublets in single-cell transcriptomic data. Cell Syst 2019;8:281–91.e9.
30. Korsunsky I, Millard N, Fan J, Slowikowski K, Zhang F, Wei K, et al. Fast, sensitive and accurate integration of single-cell data with Harmony. Nat Methods 2019;16:1289–96.
31. Becht E, McInnes L, Healy J, Dutertre CA, Kwok IWH, Ng LG, et al. Dimensionality reduction for visualizing single-cell data using UMAP. Nat Biotechnol 2018;37:38–44.
32. Ulrich BJ, Kharwadkar R, Chu M, Pajulas A, Muralidharan C, Koh B, et al. Allergic airway recall responses require IL-9 from resident memory CD4+ T cells. Sci Immunol 2022;7:eabg9296.
33. MacLean AJ, Richmond N, Koneva L, Attar M, Medina CAP, Thornton EE, et al. Secondary influenza challenge triggers resident memory B cell migration and rapid relocation to boost antibody secretion at infected sites. Immunity 2022;55:718–33.e8.
34. Gueguen P, Metoikidou C, Dupic T, Lawand M, Goudot C, Baulande S, et al. Contribution of resident and circulating precursors to tumor-infiltrating CD8+ T cell populations in lung cancer. Sci Immunol 2021;6:eabd5778.
35. Finak G, McDavid A, Yajima M, Deng J, Gersuk V, Shalek AK, et al. MAST: a flexible statistical framework for assessing transcriptional changes and characterizing heterogeneity in single-cell RNA sequencing data. Genome Biol 2015;16:278.
36. Milner JJ, Toma C, Yu B, Zhang K, Omilusik K, Phan AT, et al. Runx3 programs CD8+ T cell residency in non-lymphoid tissues and tumours. Nature 2017;552:253–7.
37. Andreatta M, Carmona SJ. UCell: robust and scalable single-cell gene signature scoring. Comput Struct Biotechnol J 2021;19:3796–8.
38. Qiu X, Mao Q, Tang Y, Wang L, Chawla R, Pliner HA, et al. Reversed graph embedding resolves complex single-cell trajectories. Nat Methods 2017;14:979–82.
39. Aibar S, González-Blas CB, Moerman T, Huynh-Thu VA, Imrichova H, Hulselmans G, et al. SCENIC: single-cell regulatory network inference and clustering. Nat Methods 2017;14:1083–6.
40. Shannon P, Markiel A, Ozier O, Baliga NS, Wang JT, Ramage D, et al. Cytoscape: a software environment for integrated models of biomolecular interaction networks. Genome Res 2003;13:2498–504.
41. Wu T, Hu E, Xu S, Chen M, Guo P, Dai Z, et al. clusterProfiler 4.0: a universal enrichment tool for interpreting omics data. Innovation (Camb) 2021;2:100141.

42. Browaeys R, Saelens W, Saeys Y. NicheNet: modeling intercellular communication by linking ligands to target genes. Nat Methods 2020;17:159–62.
43. Nardelli-Haefliger D, Dudda JC, Romero P. Vaccination route matters for mucosal tumors. Sci Transl Med 2013;5:172fs4.
44. Tan Z, Zhou J, Cheung AK, Yu Z, Cheung KW, Liang J, et al. Vaccine-elicited $CD8^+$ T cells cure mesothelioma by overcoming tumor-induced immunosuppressive environment. Cancer Res 2014;74:6010–21.
45. Clarke J, Panwar B, Madrigal A, Singh D, Gujar R, Wood O, et al. Single-cell transcriptomic analysis of tissue-resident memory T cells in human lung cancer. J Exp Med 2019;216:2128–49.
46. Yenyuwadee S, Sanchez-Trincado Lopez JL, Shah R, Rosato PC, Boussiotis VA. The evolving role of tissue-resident memory T cells in infections and cancer. Sci Adv 2022;8:eabo5871.
47. Farber DL, Yudanin NA, Restifo NP. Human memory T cells: generation, compartmentalization and homeostasis. Nat Rev Immunol 2014;14:24–35.
48. Kohlmeier JE, Miller SC, Smith J, Lu B, Gerard C, Cookenham T, et al. The chemokine receptor CCR5 plays a key role in the early memory $CD8^+$ T cell response to respiratory virus infections. Immunity 2008;29:101–13.
49. Slütter B, Pewe LL, Kaech SM, Harty JT. Lung airway-surveilling CXCR3(hi) memory $CD8^+$ T cells are critical for protection against influenza A virus. Immunity 2013;39:939–48.
50. Guo K, Yombo DJK, Wang Z, Navaeiseddighi Z, Xu J, Schmit T, et al. The chemokine receptor CXCR3 promotes $CD8^+$ T cell-dependent lung pathology during influenza pathogenesis. Sci Adv 2024;10:eadj1120.
51. Guo X, Zhang Y, Zheng L, Zheng C, Song J, Zhang Q, et al. Global characterization of T cells in non-small-cell lung cancer by single-cell sequencing. Nat Med 2018;24:978–85.
52. Curtsinger JM, Lins DC, Mescher MF. $CD8^+$ memory T cells (CD44high, Ly-6C+) are more sensitive than naive cells to (CD44low, Ly-6C-) to TCR/CD8 signaling in response to antigen. J Immunol 1998;160:3236–43.
53. Mackay LK, Rahimpour A, Ma JZ, Collins N, Stock AT, Hafon ML, et al. The developmental pathway for $CD103^+CD8^+$ tissue-resident memory T cells of skin. Nat Immunol 2013;14:1294–301.
54. Kakaradov B, Arsenio J, Widjaja CE, He Z, Aigner S, Metz PJ, et al. Early transcriptional and epigenetic regulation of $CD8^+$ T cell differentiation revealed by single-cell RNA sequencing. Nat Immunol 2017;18:422–32.
55. Poon MML, Caron DP, Wang Z, Wells SB, Chen D, Meng W, et al. Tissue adaptation and clonal segregation of human memory T cells in barrier sites. Nat Immunol 2023;24:309–19.
56. Kurd NS, He Z, Louis TL, Milner JJ, Omilusik KD, Jin W, et al. Early precursors and molecular determinants of tissue-resident memory $CD8^+$ T lymphocytes revealed by single-cell RNA sequencing. Sci Immunol 2020;5:eaaz6894.
57. Parga-Vidal L, Behr FM, Kragten NAM, Nota B, Wesselink TH, Kavazović I, et al. Hobit identifies tissue-resident memory T cell precursors that are regulated by Eomes. Sci Immunol 2021;6:eabg3533.
58. Jabri B, Abadie V. IL-15 functions as a danger signal to regulate tissue-resident T cells and tissue destruction. Nat Rev Immunol 2015;15:771–83.
59. Lin YH, Duong HG, Limary AE, Kim ES, Hsu P, Patel SA, et al. Small intestine and colon tissue-resident memory $CD8^+$ T cells exhibit molecular heterogeneity and differential dependence on Eomes. Immunity 2023;56:207–23.e8.
60. Han X, Chen H, Huang D, Chen H, Fei L, Cheng C, et al. Mapping human pluripotent stem cell differentiation pathways using high throughput single-cell RNA-sequencing. Genome Biol 2018;19:47.
61. Dadi S, Chhangawala S, Whitlock BM, Franklin RA, Luo CT, Oh SA, et al. Cancer immunosurveillance by tissue-resident innate lymphoid cells and innate-like T cells. Cell 2016;164:365–77.
62. Wahlen S, Matthijssens F, Van Loocke W, Taveirne S, Kiekens L, Persyn E, et al. The transcription factor RUNX2 drives the generation of human NK cells and promotes tissue residency. Elife 2022;11:e80320.
63. Fonseca R, Burn TN, Gandolfo LC, Devi S, Park SL, Obers A, et al. Runx3 drives a $CD8^+$ T cell tissue residency program that is absent in $CD4^+$ T cells. Nat Immunol 2022;23:1236–45.
64. Mackay LK, Wynne-Jones E, Freestone D, Pellicci DG, Mielke LA, Newman DM, et al. T-Box transcription factors combine with the cytokines TGF-beta and IL-15 to control tissue-resident memory T cell fate. Immunity 2015;43:1101–11.
65. Pan Y, Tian T, Park CO, Lofftus SY, Mei S, Liu X, et al. Survival of tissue-resident memory T cells requires exogenous lipid uptake and metabolism. Nature 2017;543:252–6.
66. Tieu R, Zeng Q, Zhao D, Zhang G, Feizi N, Manandhar P, et al. Tissue-resident memory T cell maintenance during antigen persistence requires both cognate antigen and interleukin-15. Sci Immunol 2023;8:eadd8454.
67. Wein AN, McMaster SR, Takamura S, Dunbar PR, Cartwright EK, Hayward SL, et al. CXCR6 regulates localization of tissue-resident memory CD8 T cells to the airways. J Exp Med 2019;216:2748–62.
68. Hombrink P, Helbig C, Backer RA, Piet B, Oja AE, Stark R, et al. Programs for the persistence, vigilance and control of human $CD8^+$ lung-resident memory T cells. Nat Immunol 2016;17:1467–78.
69. Sasson SC, Gordon CL, Christo SN, Klenerman P, Mackay LK. Local heroes or villains: tissue-resident memory T cells in human health and disease. Cell Mol Immunol 2020;17:113–22.
70. Myers MA, Smith AP, Lane LC, Moquin DJ, Aogo R, Woolard S, et al. Dynamically linking influenza virus infection kinetics, lung injury, inflammation, and disease severity. Elife 2021;10:e68864.
71. Masopust D, Vezys V, Wherry EJ, Barber DL, Ahmed R. Cutting edge: gut microenvironment promotes differentiation of a unique memory CD8 T cell population. J Immunol 2006;176:2079–83.
72. Veiga-Fernandes H, Walter U, Bourgeois C, McLean A, Rocha B. Response of naïve and memory $CD8^+$ T cells to antigen stimulation in vivo. Nat Immunol 2000;1:47–53.
73. Kok L, Masopust D, Schumacher TN. The precursors of $CD8^+$ tissue resident memory T cells: from lymphoid organs to infected tissues. Nat Rev Immunol 2022;22:283–93.
74. Xu Haoran, Zhou Runhong, Chen Zhiwei. Tissue-Resident Memory T Cell: Ontogenetic Cellular Mechanism and Clinical Translation. Clin Exp Immunol. 1365-2249 2023;214(3):249–259. 10.1093/cei/uxad090.